Bioconjugate Chemistry

pubs.acs.org/bc

Communication

# Trifluorinated Keto–Enol Tautomeric Switch in Probing Domain Rotation of a G Protein-Coupled Receptor

Xudong Wang, Wenjie Zhao, Sameer Al-Abdul-Wahid, Yiming Lu, Tao Cheng, Jesper J. Madsen, and Libin Ye*

Cite This: *Bioconjugate Chem.* 2021, 32, 99–105

Read Online

ACCESS | Metrics & More | Article Recommendations | Supporting Information

**ABSTRACT:** Conformational dynamics and transitions of biologically active molecules are pivotal for understanding the physiological responses they elicit. In the case of receptor activation, there are major implications elucidating disease mechanisms and drug discovery innovation. Yet, incorporation of these factors into drug screening systems remains challenging in part due to the lack of suitable approaches to include them. Here, we present a novel strategy to probe the GPCR domain rotation by utilizing the $^{19}$fluorine signal variability of a trifluorinated keto–enol (TFKE) chemical equilibrium. The method takes advantage of the high sensitivity of the TFKE tautomerism toward microenvironmental changes resulting from receptor conformational transitions upon ligand binding. We validated the method using the adenosine $A_{2A}R$ receptor as a model system in which the TFKE was attached to two sites exhibiting opposing motions upon ligand binding, namely, V229C$^{6.31}$ on transmembrane domain VI (TM6) and A289C$^{7.54}$ on TM7. Our results demonstrated that the TFKE switch was an excellent reporter for the domain rotation and could be used to study the conformational transition and dynamics of relative domain motions. Although further studies are needed in order to establish a quantitative relationship between the rotational angle and the population distribution of different components in a particular system, the research presented here provides a foundation for its application in studying receptor domain rotation and dynamics, which could be useful in drug screening efforts.

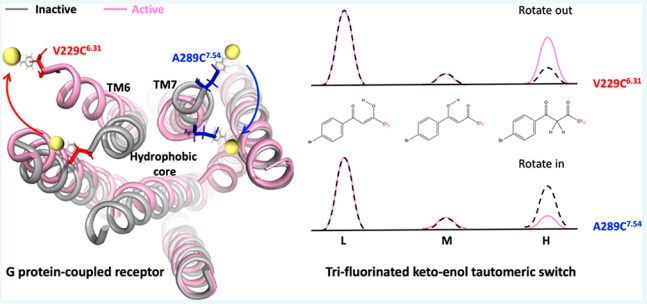




G protein-coupled receptor (GPCR), the largest membrane protein family with more than 800 members,[1] is targeted by over one-third of currently marketed drugs. At present, less than 12% of receptors have been subjected to drug discovery.[2] It is known that GPCR activation is a multistate transition process,[3] which encourages characterization of the receptor conformations and investigating the functional implications of their transitions. This has the potential to not only uncover the mechanism of receptor activation but also better design drugs to control signaling processes through fine-tuning the conformational transition and dynamics. Therefore, probing the receptor conformations in order to investigate their dynamics has become central in the post-static structural biology era. Although paramount progress has been made in the past decade, especially with the cryo-EM spectroscopy and X-ray application,[4−8] leading to more than 370 static structures[9] of over 70 GPCRs deposited in the PDB database, we are still at the very early stage of exploring the conformational transition and dynamics of the receptors. In part, this is due to methodology shortcomings and the lack of establishing a practical quantitative conformation–activity relationship for drug discovery. This suggests the opportunity to develop a strategy that can effectively probe and delineate the receptor activation process. In the last several years, emerging approaches have been explored to pursue this end. These include double electronic–electronic resonances (DEER),[10] single molecular FRET,[11] and NMR,[3,12−14] of which the NMR is one of the most powerful tools with undeniable and unique advantages to probe receptor conformations and dynamics. However, its disadvantages are also outstanding even compared to X-ray and cryo-EM spectroscopies, including insensitivity, which is especially challenging in GPCR studies because of the difficulty of heterogeneously expressing these receptors.

The fluorine nucleus has the distinction of a high gyromagnetic ratio and, thus, the greatest sensitivity for NMR, next to only tritium and $^{1}$H nuclei.[15] $^{19}$F NMR as well exhibits a distinguished range of chemical shift over hundreds of ppm,[16] in which the $^{19}$F-keto–enol family particularly exhibits a remarkable sensitivity as a single

**Received:** December 7, 2020
**Revised:** December 28, 2020
**Published:** December 30, 2020

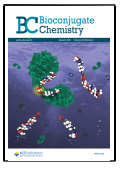





https://dx.doi.org/10.1021/acs.bioconjchem.0c00670
*Bioconjugate Chem.* 2021, 32, 99–105

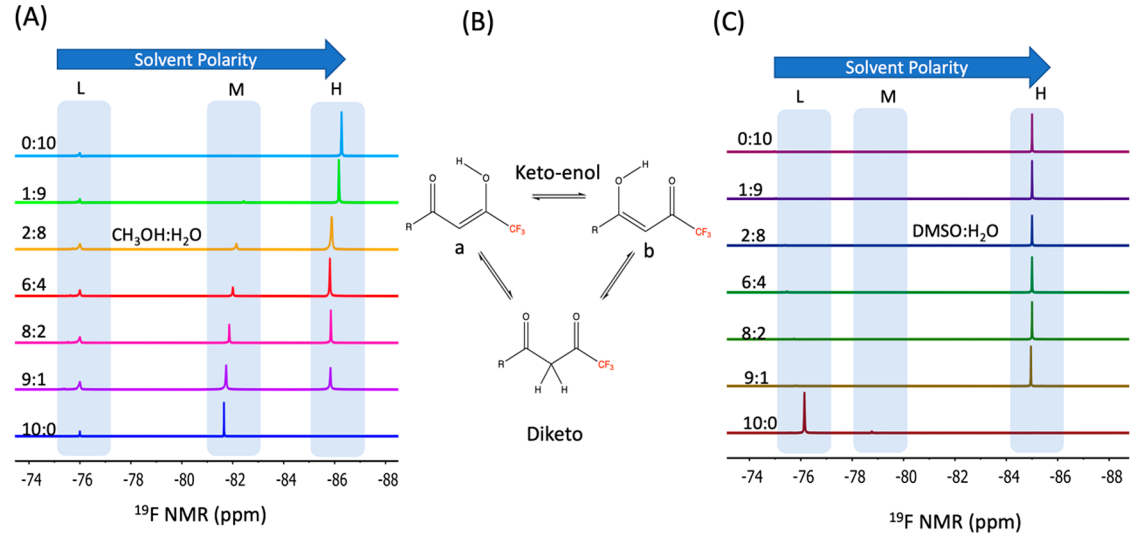


**Figure 1.** TFKE switch as a function of solvent polarity. (A) TFKE switch as a function of the mixture of $CH_3OH:H_2O$. (B) Three different isomers of TFKE switch in the solvent. (C) TFKE switch as a function of the mixture of $DMSO:H_2O$.

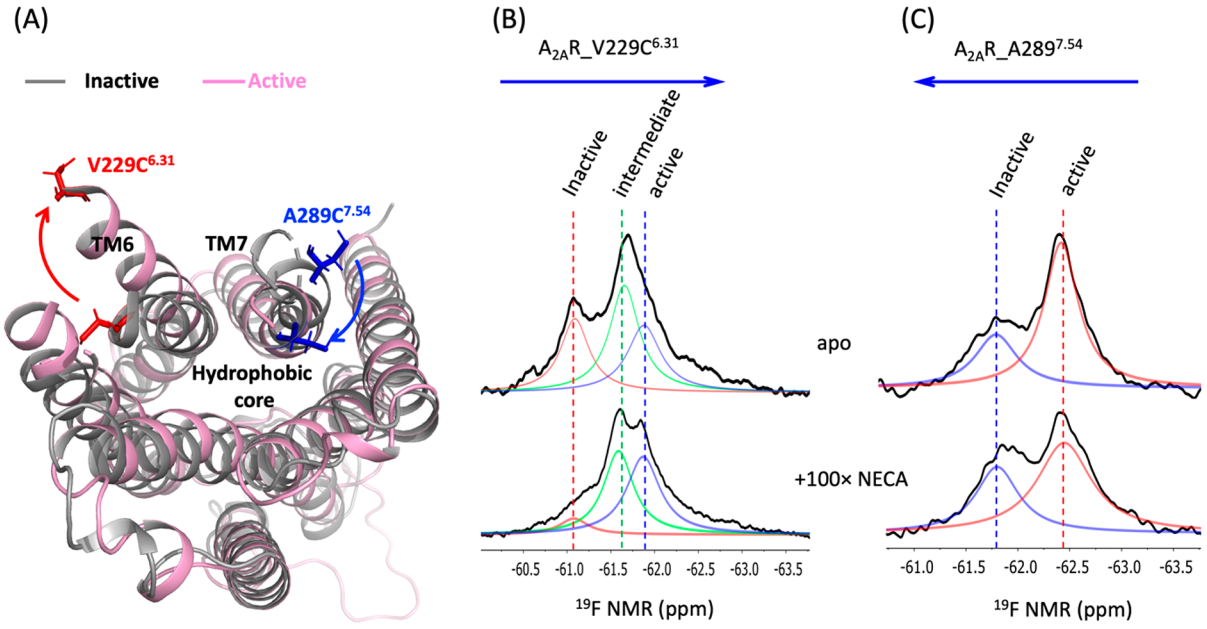


**Figure 2.** Domain rotation of TM5 and TM6 indicated by $^{19}F$ BTFMA labeled $V229C^{6.31}$ and $A289C^{7.54}$ in the $A_{2A}R$ receptor. (A) Bottom view of the $V229C^{6.31}$ and $A289C^{7.54}$ on TM6 and TM7 domains of the $A_{2A}R$ receptor (PDB ID: 2YDO). (B) $^{19}F$ NMR spectra of $^{19}F$ BTFMA labeled $V229C^{6.31}$ for apo and 100× NECA (moral ratio) saturated samples. (C) $^{19}F$ NMR spectra of $^{19}F$ BTFMA labeled $A289C^{7.54}$ for apo and 100× NECA saturated samples. Of note, the delineation of TM6 followed our previous publication while the TM7 domain simply was depicted as active and inactive components.

fluorinated species to changes in the surrounding environment. For this reason, it has been extensively reported[17−19] that structural, electronic, and solvent effects can sensitively change the keto−enol tautomeric equilibria in TFA-substituted ketones, producing enolic and keto forms with a chemical shift span of more than 16 ppm.[20] Steric deshielding of fluorine is a phenomenon that occurs when large groups (such as protein segments or domains) are in close proximity to one another due to the disturbance of the *p* orbital electrons of the fluorine atom. This motivates the development of a tactic for probing the conformational transition of the receptors by utilizing the susceptibility of the trifluorinated keto−enol (TFKE) to the microenvironmental changes.

## RESULTS AND DISCUSSION

**Susceptibility of TFKE Switch to Microenvironmental Change.** To explore the TFKE switch profile in response to the microenvironmental changes, we started with two solvent systems of different polarities consisting of a $CH_3OH:H_2O$ or $DMSO:H_2O$ mixture in order to monitor the TFKE tautomeric transition. As shown in Figure 1A and C, a series of $^{19}F$ NMR spectra as a function of $CH_3OH:H_2O$ or $DMSO:H_2O$ mixtures were acquired. Three $^{19}F$ signals were distinctly observed in the spectra in both cases, corresponding to the keto−enol structures and equilibria shown in Figure 1B. The assignments of each peak were determined in reference to the previous publications,[3,21−23] in which peak H at −85.4


https://dx.doi.org/10.1021/acs.bioconjchem.0c00670
Bioconjugate Chem. 2021, 32, 99−105

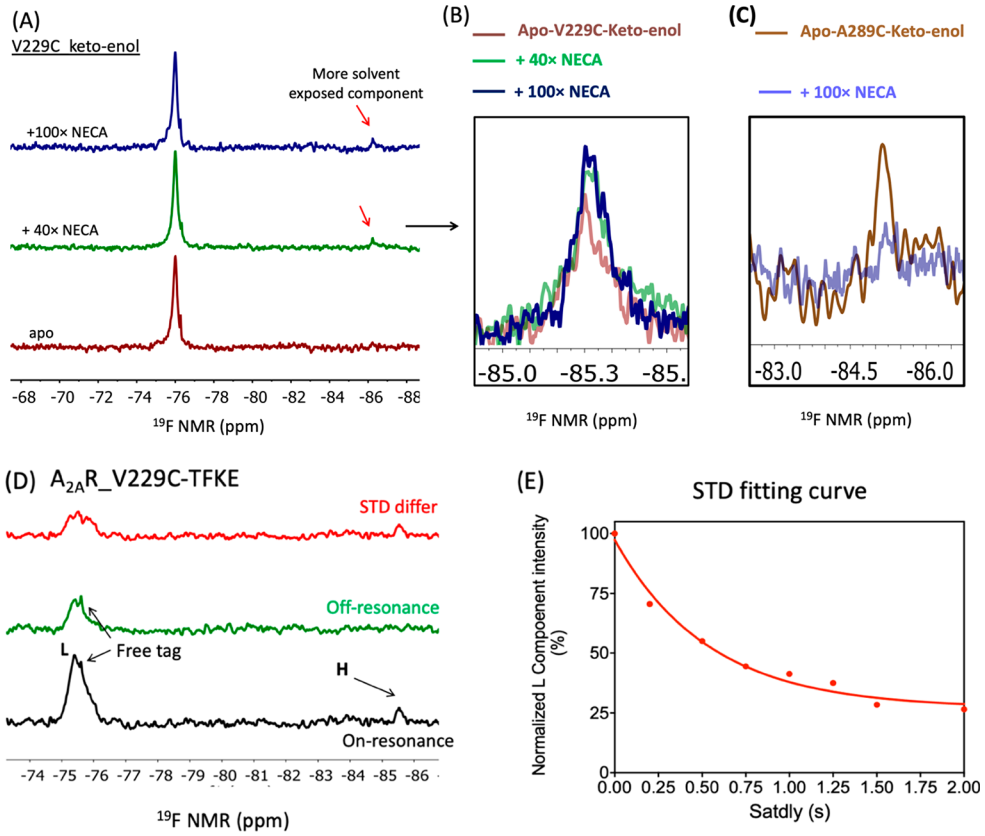


**Figure 3.** Domain rotations and dynamics of the $A_{2A}R$ probed by TFKE switch using $V229C^{6.31}$ and $A289C^{7.54}$ as probing sites. (A) $^{19}F$ NMR spectra of TFKE labeled $V229C^{6.31}$ as a function of agonist NECA. (B) Highlighted H components from $^{19}F$ NMR spectra of TFKE labeled $V229C^{6.31}$. (C) Highlighted H components from $^{19}F$ NMR spectra of TFKE labeled $A289C^{7.54}$. (D) Saturation transfer difference (STD) for TFKE labeled $A_{2A}R$-V229C, in which on-resonance, off-resonance, and STD spectra are shown in different colors. (E) Saturation transfer experiments as a function of different mixture times from 0 through 2 s.

ppm on the high magnetic field was a component with a highly hydrophilic property, while the middle peak M had the medium characteristics and the left-most peak L at −76.0 ppm was at least hydrophilic (the most hydrophobic component), referenced to the polarities of DMSO, $CH_3OH$, and $H_2O$ were 0.444 (least), 0.762 (medium), and 1.000, respectively (DOI: 10.18434/T4D303). The assignment was also deduced by $^{19}F$ chemical shift prediction using software Mestrenova, as shown in SI Figure S1, as well as previous publications, in which ∼ −86 ppm peak H was identified as a hydrated form of the diketone with high hydrophilic feature,[21,22,23] while resonances L and M were time-averaged keto−enol tautomer signals with different hydration extents, in which the L component with propensity of forming the "a" form and the M component with propensity of forming the "b" form are found. Both of them resulted from an equilibrium dependent on the tautomerization exchange. It is also noted that the ethyl acetal form of the diketone also has a similar chemical shift around ∼85 ppm,[21,23] though it is not discussed in this study. It is obvious that the microenvironmental changes caused by the receptor domain transition would not merely be affected by the microenvironmental polarity changes but also affected by the electrostatic variations, which result from deshielding the $^{19}F$ groups when forming polar interactions with domain segments.[24] Therefore, the keto−enol system is promising in probing conformational transition via shielding and deshielding effects elicited by ligand binding to the receptor, which leads to movements of domain segments and alters the electrostatic cloud surrounding the trifluorinated probe. To validate this, a well-established $A_{2A}R$ adenosine receptor system available in our lab was used.

**Topological Rotations of the Sites of $V229C^{6.31}$ and $A289C^{7.54}$ upon Receptor Activation.** It is a common structural feature of GPCR activation, as indicated by many resolved structures such as $\beta_2$AR,[25] CGRP,[5] CTR,[6] GLP-1R,[7] CB1 and CB2,[26] CXCL8,[27] and parathyroid hormone receptor type 1[28] in comparison to their inactive structures, that the concerted movement of transmembrane helices: TM6 domain leaves the hydrophobic core of the heterotrimeric G protein binding cavity by rotating out; the TM7 domain is packed inward toward the core of the cavity; the TM5 domain protrudes. This structural feature indicates that the TM6 and TM7 domains are inversely operated in reference to the G protein binding cavity upon the ligand binding. Therefore, by using these two domains as the probing sites, we should be able to measure the opposing motions. Previously, we have successfully explored the site of $V229C^{6.31}$ (Figure 2A) on the TM6 domain, which was rotated away from the hydrophobic core upon the receptor activation. This was shown by a high-field component (active conformations) of $^{19}F$ chemical shift was populated at the expense of low chemical field components (inactive conformations) in the BTFMA conjugated receptor. To better validate the application of TFKE in probing the conformational transition upon the receptor activation, a second site was also exploited on the TM7 domain that exhibits the opposing motion compared with the $V229C^{6.31}$


https://dx.doi.org/10.1021/acs.bioconjchem.0c00670
Bioconjugate Chem. 2021, 32, 99−105

site. According to the chemical shift prediction using the PROSHIFT,[29] the site of A289C$^{7.54}$ on the TM7 domain was identified. We proposed that the low-field component (active conformation), the counterpart to the high field component of the TM6, should be further populated when the receptor was activated. Indeed, this component was increased upon the binding of full agonist NECA (Figure 2C) as expected. Thus, we have established a system with two labeling sites that can properly probe the individual rotations of TM6 and TM7 domains of the $A_{2A}R$ receptor. In this system, we predict that the H component in the $^{19}F$ spectra of keto−enol attached to the site of V229C$^{6.31}$ would be accumulated when the receptor is activated, whereas its population would decrease when the probe is attached to the A289C$^{7.54}$ site.

**The H Component in the TFKE Switch Is an Indicator of Domain Rotation.** According to the rationale established in the previous section, we labeled $A_{2A}R$_V229C$^{6.31}$ and $A_{2A}R$_A289C$^{7.54}$ with the TFKE compound to examine the conformational transition of the $A_{2A}R$ activation as delineated by the TFKE switch. We expected that the hydrophilic component H should increase in the case of V229C$^{6.31}$ upon receptor activation, while the corresponding population should decrease in the case of A289C$^{7.54}$. The receptor purification follows our previously established protocol[3,30] with slight modifications as a result of the keto−enol labeling (see the Method and Materials section for details). The purity and functionality of the purified receptors were verified by SDS-PAGE (SI Figure S2) and radioligand binding assay (SI Figure S3), respectively. We saturated the keto−enol-labeled receptors with agonist NECA to examine whether the conversions among L, M, and H components were qualitatively aligned with our previous results where the BTFMA tag was used. As shown in Figure 3A, the addition of 40× agonist NECA in molar ratio (same as described below unless otherwise specified) indeed led to a ∼17% population increase of component H in comparison to its occupancy in apo state, indicating the site of V229C$^{6.31}$ was more solvent accessible resulting from out-rotating of the TM6 domain when the receptor was activated. In contrast, the addition of full agonist NECA to the $A_{2A}R$_A289C$^{7.54}$ resulted in a dramatic decrease of the H component (around 66%) because the TM7 domain was approaching the hydrophobic core of the receptor upon activation. Of note, the increased percentage of V229C$^{6.31}$ was significantly smaller than that of A289C$^{7.54}$ in part due to the effect of DMSO used for dissolving the ligand NECA as shown in SI Figure S4. Therefore, we can conclude the component H is an excellent indicator for probing the GPCR domain rotation and we expect it is broadly applicable to other proteins of interest (POIs).

In contrast to other $^{19}F$ probes (e.g., BTFMA), the receptor conjugation leads to line width broadening because of the increase of the rotational correlation time ($\tau_c$) of the protein conjugated $^{19}F$ probe, resulting from the particle-size increase in comparison with the free tag. This may further shorten the T2 value and broaden NMR signals, potentially impairing the application of $^{19}F$ NMR in probing the dynamics of individual conformational states. However, as we see for the trifluorinated keto−enol, the components L, M, and H are naturally separated without overlap, making it possible to study the different components and accompanying conformational transitions.

Furthermore, the current state-of-the-art 19-fluorinated probe setup (BTFMA)[3,15,31] can only dissect the receptor ensemble into four conformations, in which only two resonances can be visibly distinguished without the assistance of spectral deconvolution. In contrast, the keto−enol system intrinsically has three physical moieties and therefore potentially the capacity to distinguish three conformational states (L represents the most hydrophobic component; H represents the most hydrophilic component; M represents a state in the middle). Unfortunately, we did not observe the M component in this study, which might be related to the overall detergent system's hydrophobicity as indicated in Figure 1.

**Conformational Transition of GPCR Probed by Saturated Transfer Difference.** In the study using BTFMA for probing the receptor conformational transition, one difficulty is to accurately distinguish various conformers due to the severe spectral overlap among different conformations, indicated in Figure 2. In contrast, using the TFKE equilibrium system, components L, M, and H are physically separated, facilitating the dynamics and conformational transition study between these different components. The three intrinsic components of the keto−enol system will in principle deliver receptor conformations categorized into the three conformers, in which the L represents the most hydrophobic conformer, while the H represents the most hydrophilic conformer and the M represents the in-between conformer. Meanwhile, the subconformers could be further delineated within each category in some cases. Therefore, the transition of these components can be examined without interference from spectral overlap. As shown in Figure 3D, saturation transfer difference experiments indicated the exchange between L and H components, whose exchange rate can be measured by applying a series of saturation pulses on the active component of H and fitting into the equation listed in the method as shown in Figure 3E. Note that there was a free tag identified through pulse CPMG (SI Figure S5), in which the bound peak decayed rapidly because of exchange between different conformations, while the resonance for the free peak was outstanding due to the absence of component exchange or an out-of-range exchange rate in the time-regime of CPMG.

## CONCLUSION AND DISCUSSION

Conformational transitions and their associated dynamics have become essential in understanding structural biology and gaining insights into the mechanisms of physiological receptors. The approach presented here takes advantage of the high environmental sensitivity of TFKE and provides an additional useful tool to study the conformational transitions through specific domain rotations. As indicated in Figure 1, the NMR profiles showed that the population ratios between different components in the TFKE switch are polarity-dependent, which can be further explored for establishing a population matrix for a particular receptor in a given solvent system. We systematically investigated the effects of the MNG-3 concentration in the solvent system on the TFKE component profile (SI Figure S6). The data indicated that the solvent system affected the proportional distribution[32] between the three components corresponding to the three tautomers. The solvent system selection is important for any particular study in order to interrogate the conformational transitions and domain rotations for a quantitative correlation between ligand functionality and the TFKE component populations.


https://dx.doi.org/10.1021/acs.bioconjchem.0c00670
Bioconjugate Chem. 2021, 32, 99−105

It is worthy of note that the TFKE probe has a better resolution than the $^{19}F$ probe—BTFMA in terms of the separation among different components—the resolution of H, M, and L in the keto−enol equilibrium (Figure 1 and Figure 3) versus inactive, intermediate, and active components in the BTFMA (Figure 2). Based on this, it should be easier to study dynamics and conformational transition among H, M, and L than the corresponding transitions using BTFMA. However, we would also like to point out that the conformations probed by these two probes are different and not in 1-to-1 correspondence. Recall that the receptor conformations were restrained into two/three components in the TFKE case, while there were no restraints in BTFMA case, though its resolution was much worse than that of TFKE and highly relied on the spectral deconvolution. Therefore, we suggest using TFKE to probe the local domain rotation (via the H component) instead of accurately quantifying receptor-active, intermediate, and inactive conformations.

## METHODS AND MATERIALS

**$^{19}F$ NMR of the Free Keto−Enol in Mixtures of $CH_3OH$:$H_2O$ and DMSO:$H_2O$.** A series of MeOH/water or DMSO/water mixtures were prepared, ranging from MeOH/water (v/v) 10:0 through 0:10, as shown in Figure 1. NMR experiments were performed on a Bruker neo600 MHz ($^1H$ Larmor frequency) spectrometer equipped with a Smartprobe capable for $^{19}F$ NMR acquisition with a S/N 1200. All experiments were performed at 20 °C with transmitter frequency set to −60.0 ppm and spectrum width of 60 ppm.

**$A_{2A}R$ Receptor Expression and Purification.** A single yeast colony on YPD plates was used to inoculate 4 mL of YPD medium and then grow for 12 h. Subsequently, the culture was used to inoculate 200 mL of BMGY medium (1% (w/v) yeast extract, 2% (w/v) peptone, 1.34% (w/v) YNB (yeast nitrogen base) without amino acids, 0.00004% (w/v) biotin, 1% (w/v) glycerol, and 0.1 M PB (phosphate buffer at pH 6.5) and grown for an additional 24 h. Cells were spun down and resuspended in 1 L of BMMY medium (1% (w/v) yeast extract, 2% (w/v) peptone, 1.34% (w/v) YNB without amino acids, 0.00004% (w/v) biotin, 0.5% (w/v) methanol, 0.1 M phosphate buffer at pH 6.5, 0.04% (w/v) histidine and 3% (v/v) DMSO, 10 mM theophylline) at 20 °C. Methanol (0.5% (v/v)) was added every 12 h. Sixty hours after induction, yeast cells were harvested.

Cell pellets were collected by centrifugation and washed with 50 mM HEPES, 10% glycerol, pH 7.4 before the addition of breaking buffer (50 mM HEPES, pH 7.4, 100 mM NaCl, 2 mM EDTA, 10% glycerol, 100 μM theophylline). The homogenized cell pellets were applied to LM20 Microfluidizer for disrupting the yeast cell walls and releasing the membrane fraction parts. Note that the temperatures were consistently kept at 4 °C by placing the sample in an ice−water bath, and the disruption pressure was set to 15,000 psi. Four passages of disruption were conducted in order to maximize the membrane release and as such increased the receptor production. Undisrupted yeast cells and cell debris were separated from the membrane suspension by centrifugation at 8000 × g for 30 min. The supernatant was then collected and centrifuged at 100,000 × g for 1 h, and the precipitated cell membranes were immediately dissolved in 50 mM HEPES, pH 7.4, 100 mM NaCl, 1% MNG-3 (lauryl maltose neopentyl glycol), and 0.02% CHS (cholesteryl hemisuccinate), 100 μM theophylline, and 20 mM imidazole under continuous agitation for 1−2 h at 4 °C until the solution was transparent. Subsequently, Talon resin (Clontech) was added to the solubilized membranes and incubated for 2 h. The $A_{2A}R$-bound Talon resin was washed with 50 mM HEPES buffer, pH 7.4, containing 100 mM NaCl, 0.1% MNG-3, and 0.02% CHS and resuspended in the same buffer, followed by addition of 100 μM TCEP reducing agent and incubation for 20 min. TCEP was washed out immediately with a buffer consisting of 50 mM HEPES, pH 7.4, 100 mM NaCl, 0.1% MNG-3, and 0.02% CHS. The $A_{2A}R$-bound Talon resin was then resuspended in 50 mM HEPES, pH 7.4, 100 mM NaCl, 0.1% MNG-3, and 0.02% CHS, and combined with the BTFMA.[15] While $A_{2A}R$ was bound to a Talon (metal affinity) resin via the C-terminal poly-HIS tag, the N-terminal FLAG tag was removed via tobacco etch virus (TEV) protease. After its removal, the $A_{2A}R$-bound Talon resin was extensively washed, using a disposable column, with 50 mM HEPES, pH 7.4, 100 mM NaCl, 0.1% MNG-3, and 0.02% CHS. Apo-$A_{2A}R$ was then eluted from the Talon resin with 50 mM HEPES, pH 7.4, 100 mM NaCl, 0.1% MNG-3, 0.02% CHS, and 250 mM imidazole. Sodium chloride and imidazole in the sample were removed by dialysis against 50 mM HEPES, pH 7.4, 0.1% MNG-3, and 0.02% CHS for 3 h. The XAC-agarose gel (antagonist xanthine amine congener (XAC) conjugated to Affi-Gel 10 resin) and $A_{2A}R$ were subsequently incubated together for 2 h with gentle nutation. Functional $A_{2A}R$ was eluted with 50 mM HEPES, pH 7.4, 0.1% MNG-3, 0.02% CHS, 100 mM NaCl, and 20 mM theophylline. Talon resin was added to the eluted sample and incubated for another 2 h to bind functional $A_{2A}R$. Conjugated $A_{2A}R$ was washed extensively with 50 mM HEPES, pH 7.4, 100 mM NaCl, 0.1% MNG-3, 0.02% CHS, and 20 mM imidazole, to remove all theophylline. The functional apo-$A_{2A}R$ was eluted with 50 mM HEPES, pH 7.4, 100 mM NaCl, 0.1% MNG-3, 0.02% CHS, and 250 mM imidazole, and the sample was dialyzed to remove imidazole for NMR experiments.

**Labeling and $^{19}F$ NMR Experiments for Receptor.** The $^{19}F$ labeling for NMR experiments was conducted during the purification procedure at the step when the receptor was conjugated onto the Talon resin. The BTFMA and fluorinated keto−enol reagent were added into the solution with an estimated concentration of 20 times that of the receptor. The second addition was conducted after 12 h and labeling continued overnight. The free tag was washed away using the buffer consisting of 50 mM HEPES, pH 7.4, 100 mM NaCl, 0.1% MNG-3, and 0.02% CHS.

NMR samples consisted of 250 μL volumes of BTFMA or keto−enol labeled 50 μM $A_{2A}R\_V229C^{6.31}$ and $A_{2A}R\_A289C^{7.54}$ in 50 mM HEPES buffer and 100 mM NaCl, doped with 10% $D_2O$ as well as 10 μL bendroflumethiazide as an internal reference. All $^{19}F$ NMR experiments were performed on a Bruker neo 600 MHz spectrometer equipped with a Smartprobe with the high-frequency channel tunable to $^{19}F$ at 20 °C. The typical 1D $^{19}F$ NMR experimental setup included a 12 μs 90° excitation pulse, an acquisition time of 250 ms, a spectral width of 15 kHz, and a repetition time of 1 s. Most spectra were acquired with 10,000 scans depending on sample concentrations. The deconvolutions of $^{19}F$ NMR spectra were performed using the software MestReNova 12.0.3 as described in detail in our previous publication.[3]

**SDS-PAGE.** In order to verify the purity of the prepared receptor, the SDS-PAGE was performed as follows: 10 μL of TFKE labeled $A_{2A}R\_V229C^{6.31}$ and $A_{2A}R\_A289C^{7.54}$ premixed with 10 μL 2× loading buffer from 50 mL stock consisting of


https://dx.doi.org/10.1021/acs.bioconjchem.0c00670
Bioconjugate Chem. 2021, 32, 99−105

12.5 mL 4 × Tris, pH 6.8, 2.5 mL 10% SDS, 5 mL 100% glycerol, and 1 mg bromophenol blue. The mixtures were incubated at room temperature for 1 h without heating before running the gel. Typically, a 15 μL mixture for each sample was subjected to the gel and the running condition was 120 V for 90 min. The gel was then first fixed 50% methanol/10% acetate acid for 5 min, followed with staining by Coomassie G-250 for 2 h prior to destaining with 40% methanol/10% acetate acid multiple times until the background was removed. The destained gel was finally photographed using the Biorad ChemiDoc MP imaging system.

**Radioligand Binding Assay.** In order to ensure the functionality of the receptor prior to large-scale receptor preparation, radioligand binding assay (saturation binding assay) was performed to exclude nonfunctional cysteine-minimized mutants. In brief, the collected cell membranes from yeast culture that contained different mutants incubated with different concentrations of [3H]CGS21680 for 2 h at 20 °C. For the nonspecific binding, 1 μL of 10 μM cold ligand CGS21680 was added to the samples. Free radioligand was separated from bound radioligand by rapid filtration onto a Whatman GF/C filter pretreated with 0.2% polyethylenimine using Millipore XX2702550 12 Position Vacuum Filtration Sampling Manifold. Radioligand activity was measured by liquid counting using LS 6500 Multi-Purpose Scintillation Counter. A minimum of three independent experiments was performed, and the values were pooled to generate the mean curves. Meanwhile, the functionality of the receptor was monitored through the whole receptor preparation procedure prior to NMR experiments. Of note, the functionality of all labeled receptors was likewise measured using the same procedure.

**$^{19}$F Saturation Transfer Experiments.** To study the exchanges between components, $^{19}$F chemical exchange saturation transfer NMR experiments were conducted. A series of continuous-wave irradiation pulses were applied on an on-resonance frequency of component H at 14,469.0 Hz with varied sat delay mixture time from 0 to 2 s. The satpwr was set to −3. An off-resonance frequency was also used in order to acquire a reference spectrum, in which the frequency was set to 12,633.0 Hz. Upon saturating the resonance associated with component H, the ideal magnetization response of component L may be described by the following formula:[33] $M_t^A = M_0^A[(k_{AB}/(\rho_A + k_{AB}))\exp[-\tau((\rho_A + k_{AB}) + \rho_A/(\rho_A + k_{AB})]$, if an exchange rate needs to be determined, in which off-resonant effects are accounted for. Note that both the exchange rate constants, $k_{AB}$, and the longitudinal relaxation rate of spin A, $\rho_A$, can in principle be calculated from a fit the above equation to the experiment data. Accordingly, the lifetime $\tau_A$ can be easily calculated from $\tau = 1/k_{AB}$. The fitting can be performed using Gnuplot (http://www.gnuplot.info).

## ■ ASSOCIATED CONTENT

### Supporting Information

The Supporting Information is available free of charge at https://pubs.acs.org/doi/10.1021/acs.bioconjchem.0c00670.

$^{19}$F NMR Chemical shift predictions for TFKE tautomers in TFKE equilibrium using Mestrenova prediction software; SDS-PAGE of purified TFKE conjugated $A_{2A}$R_V229C and $A_{2A}$R_A289C; Radioligand binding assays for $A_{2A}$R_V229C and $A_{2A}$R_A289C; The effects of DMSO used for the ligand preparations on the profiles of L, M, and H components; CPMG spectra used for distinguishing the conjugated and nonconjugated TFKE probes; TFKE equilibrium as a function of MNG-3 concentrations (PDF)

## ■ AUTHOR INFORMATION


### Corresponding Author

**Libin Ye** − *Department of Cell Biology, Microbiology and Molecular Biology, University of South Florida, Tampa, Florida 33620, United States; H. Lee Moffitt Cancer Center & Research Institute, Tampa, Florida 33612, United States;* orcid.org/0000-0003-0818-2972; Phone: 1-813-974-6007; Email: libinye@usf.edu

### Authors

**Xudong Wang** − *Department of Cell Biology, Microbiology and Molecular Biology, University of South Florida, Tampa, Florida 33620, United States*

**Wenjie Zhao** − *Department of Cell Biology, Microbiology and Molecular Biology, University of South Florida, Tampa, Florida 33620, United States*

**Sameer Al-Abdul-Wahid** − *Nuclear Magnetic Resonance Center, University of Guelph, Guelph, Ontario NIG2W1, Canada;* orcid.org/0000-0001-7925-5863

**Yiming Lu** − *Institute of Functional Nano&Soft Materials, Soochow University, Suzhou, Jiangsu 215123, China*

**Tao Cheng** − *Institute of Functional Nano&Soft Materials, Soochow University, Suzhou, Jiangsu 215123, China*

**Jesper J. Madsen** − *Department of Global Health, College of Public Health, University of South Florida, Tampa, Florida 33612, United States;* orcid.org/0000-0003-1411-9080

Complete contact information is available at: https://pubs.acs.org/10.1021/acs.bioconjchem.0c00670


### Author Contributions

L.Y. conceived the idea and wrote the manuscript. X.W. performed receptor expression, purification, labeling and NMR acquisition and analyses. W.Z. performed the $^{19}$F NMR of the free TFKE in mixtures of $CH_3OH$:$H_2O$ and DMSO:$H_2O$ acquisition and analyses. S.A.W. assisted the NMR acquisition and analyses. Y.L., T.C., and J.J.M. were involved in chemical shift prediction. All authors were involved in the discussion and manuscript revisions. L.Y. supervised the whole project.

### Notes

The authors declare no competing financial interest.

## ■ ACKNOWLEDGMENTS

We thank support from the Nexus Initiative (L.Y.) Award from University of South Florida (USF) as well as startup funding (L.Y.) from the department of Cell Biology, Microbiology and Molecular Biology at USF.

## ■ REFERENCES


(1) Takeda, S., Kadowaki, S., Haga, T., Takaesu, H., and Mitaku, S. (2002) Identification of G protein-coupled receptor genes from the human genome sequence. *FEBS Lett. 520*, 97−101.

(2) Sriram, K., and Insel, P. A. (2018) GPCRs as targets for approved drugs: How many targets and how many drugs? *Mol. Pharmacol. 93*, 251.

(3) Ye, L., Van Eps, N., Zimmer, M., Ernst, O. P., and Prosser, R. S. (2016) Activation of the $A_{2A}$ adenosine G-protein-coupled receptor by conformational selection. *Nature 533*, 265−268.

(4) Rasmussen, S. G. F., DeVree, B. T., Zou, Y. Z., Kruse, A. C., Chung, K. Y., Kobilka, T. S., Thian, F. S., Chae, P. S., Pardon, E., Calinski, D., et al. (2011) Crystal structure of the $\beta_2$ adrenergic receptor-Gs protein complex. *Nature 477*, 549−555.
(5) Liang, Y. L., Khoshouei, M., Deganutti, G., Glukhova, A., Koole, C., Peat, T. S., Radjainia, M., Plitzko, J. M., Baumeister, W., Miller, L. J., et al. (2018) Cryo-EM structure of the active, Gs-protein complexed, human CGRP receptor. *Nature 561*, 492−497.
(6) Liang, Y.-L., Khoshouei, M., Radjainia, M., Zhang, Y., Glukhova, A., Tarrasch, J., Thal, D. M., Furness, S. G. B., Christopoulos, G., Coudrat, T., et al. (2017) Phase-plate cryo-EM structure of a class B GPCR-G-protein complex. *Nature 546*, 118−123.
(7) Liang, Y. L., Khoshouei, M., Glukhova, A., Furness, S. G. B., Zhao, P., Clydesdale, L., Koole, C., Truong, T. T., Thal, D. M., Lei, S., et al. (2018) Phase-plate cryo-EM structure of a biased agonist-bound human GLP-1 receptor-Gs complex. *Nature 555*, 121−125.
(8) Zhang, Y., Sun, B., Feng, D., Hu, H., Chu, M., Qu, Q. H., Tarrasch, J. T., Li, S., Kobilka, T. S., Kobilka, B. K., et al. (2017) Cryo-EM structure of the activated GLP-1 receptor in complex with a G protein. *Nature 546*, 248−253.
(9) Congreve, M., de Graaf, C., Swain, N. A., and Tate, C. G. (2020) Impact of GPCR structures on drug discovery. *Cell 181*, 81−91.
(10) Wingler, L. M., Elgeti, M., Hilger, D., Latorraca, N. R., Lerch, M. T., Staus, D. P., Dror, R. O., Kobilka, B. K., Hubbell, W. L., and Lefkowitz, R. J. (2019) Angiotensin analogs with divergent bias stabilize distinct receptor conformations. *Cell 176*, 468−478.
(11) Gregorio, G. G., Masureel, M., Hilger, D., Terry, D. S., Juette, M., Zhao, H., Zhou, Z., Perez-Aguilar, J. M., Hauge, M., Mathiasen, S., et al. (2017) Single-molecule analysis of ligand efficacy in $\beta$2AR-G-protein activation. *Nature 547*, 68−73.
(12) Casiraghi, M., Damian, M., Lescop, E., Point, E., Moncoq, K., Morellet, N., Levy, D., Marie, J., Guittet, E., Baneres, J. L., et al. (2016) Functional modulation of a G protein-coupled receptor conformational landscape in a lipid bilayer. *J. Am. Chem. Soc. 138*, 11170−5.
(13) Ye, L., Neale, C., Sljoka, A., Lyda, B., Pichugin, D., Tsuchimura, N., Larda, S. T., Pomes, R., Garcia, A. E., Ernst, O. P., et al. (2018) Mechanistic insights into allosteric regulation of the $A_{2A}$ adenosine G protein-coupled receptor by physiological cations. *Nat. Commun. 9*, 1372.
(14) Horst, R., Liu, J. J., Stevens, R. C., and Wuthrich, K. (2013) $\beta$2-adrenergic receptor activation by agonists studied with $^{19}$F NMR spectrosc. *Angew. Chem., Int. Ed. 52*, 10762−5.
(15) Ye, L., Larda, S. T., Frank Li, Y. F., Manglik, A., and Prosser, R. S. (2015) A comparison of chemical shift sensitivity of trifluoromethyl tags: optimizing resolution in $^{19}$F NMR studies of proteins. *J. Biomol. NMR 62*, 97−103.
(16) Danielson, M. A., and Falke, J. J. (1996) Use of $^{19}$F NMR to probe protein structure and conformational changes. *Annu. Rev. Biophys. Biomol. Struct. 25*, 163−95.
(17) Matwijczuk, A., Karcz, D., Walkowiak, R., Furso, J., Gladyszewska, B., Wybraniec, S., Niewiadomy, A., Karwasz, G. P., and Gagos, M. (2017) Effect of solvent polarizability on the keto/enol equilibrium of selected bioactive molecules from the 1,3,4-thiadiazole group with a 2,4-hydroxyphenyl function. *J. Phys. Chem. A 121*, 1402−1411.
(18) Ferrari, E., Saladini, M., Pignedoli, F., Spagnolo, F., and Benassi, R. (2011) Solvent effect on keto-enol tautomerism in a new e-diketone: a comparison between experimental data and different theoretical approache. *New J. Chem. 35*, 2840−2847.
(19) Sloop, J., Bumgardner, C., Washington, G., Loehle, W. D., Sankar, S. S., and Lewis, A. B. (2006) Keto-enol and enol-enol tautomerism in trifluoromethyl-$\beta$-diketones. *J. Fluorine Chem. 127*, 780−786.
(20) Sloop, J. (2013) 19-Fluorine nuclear magnetic resonance chemical shift variability in trifluoroacetyl species. *Rep. Org. Chem. 3*, 1−12.
(21) Salman, S. R., Farrant, R. D., and Lindon, J. C. (1990) Multinuclear magnetic resonance study of tautomerism in fluoriniated 1-diketones. *Magn. Reson. Chem. 28*, 645−650.
(22) Sloop, J. (2013) 19-Fluorine nuclear magnetic resonance chemical shift variability in trifluoroacetyl species. *Rep. Org. Chem. 3*, 1−12.
(23) Sloop, J., Churley, M., Guzman, A., Moseley, S., Stalker, S., Weyand, J., and Yi, J. (2014) Synthesis and reactivity of fluorinated cyclic ketones: initial findings. *Am. J. Org. Chem. 1*, 1−10.
(24) Lingel, A., Vulpetti, A., Reinsperger, T., Proudfoot, A., Denay, R., Frommlet, A., Henry, C., Hommel, U., Gossert, A. D., and Luy, B. (2020) Comprehensive and high-throughput exploration of chemical space using broadband $^{19}$F NMR-based screening. *Angew. Chem., Int. Ed. 59*, 14698.
(25) Rasmussen, S. G. F., DeVree, B. T., Zou, Y., Kruse, A. C., Chung, K. Y., Kobilka, T. S., Thian, F. S., Chae, P. S., Pardon, E., Calinski, D., et al. (2011) Crystal structure of the $\beta_2$ adrenergic receptor-Gs protein complex. *Nature 477*, 549−555.
(26) Hua, T., Li, X., Wu, L., Iliopoulos-Tsoutsouvas, C., Wang, Y., Wu, M., Shen, L., Johnston, C. A., Nikas, S. P., Song, F., et al. (2020) Activation and signaling mechanism revealed by cannabinoid receptor-Gi complex structures. *Cell 180*, 655−665.
(27) Liu, K., Wu, L., Yuan, S., Wu, M., Xu, Y., Sun, Q., Li, S., Zhao, S., Hua, T., and Liu, Z. J. (2020) Structural basis of CXC chemokine receptor 2 activation and signalling. *Nature 585*, 135−140.
(28) Zhao, L. H., Ma, S., Sutkeviciute, I., Shen, D. D., Zhou, X. E., de Waal, P. W., Li, C. Y., Kang, Y. Y., Clark, L. J., et al. (2019) Structure and dynamics of the active human parathyroid hormone receptor-1. *Science 364*, 148−153.
(29) Meiler, J. (2003) PROSHIFT: protein chemical shift prediction using artificial neural networks. *J. Biomol. NMR 26*, 25−37.
(30) Ye, L., Orazietti, A. P., Pandey, A., and Prosser, R. S. (2018) High-efficiency expression of yeast-derived G-protein coupled receptors and $^{19}$F labeling for dynamical studies. *Methods Mol. Biol. 1688*, 407−421.
(31) Manglik, A., Kim, T. H., Masureel, M., Altenbach, C., Yang, Z., Hilger, D., Lerch, M. T., Kobilka, T. S., Thian, F. S., Hubbell, W. L., et al. (2015) Structural insights into the dynamic process of.2-adrenergic receptor signaling. *Cell 161*, 1101−1111.
(32) Ferrari, E., Saladini, M., Pignedoli, F., Spagnolo, F., and Benassi, R. (2011) Solvent effect on keto-enol tautomerism in a new $\beta$-diketone: a comparison between experimental data and different theoretical approaches. *New J. Chem. 35*, 2840−2847.
(33) Helgstrand, M., Hard, T., and Allard, P. (2000) Simulations of NMR pulse sequences during equilibrium and non-equilibrium chemical exchange. *J. Biomol. NMR 18*, 49−63.


https://dx.doi.org/10.1021/acs.bioconjchem.0c00670
*Bioconjugate Chem.* 2021, 32, 99−105